JBC Papers in Press. Published on January 21, 2007 as Manuscript M609552200
The latest version is at http://www.jbc.org/cgi/doi/10.1074/jbc.M609552200

Critical Role for Polar Residues in Coupling Leukotriene B_4 Binding to Signal Transduction in BLT1

Sudeep Basu[1,2], Venkatakrishna R. Jala[1], Steven Mathis[1,2], Soujanya T. Rajgopal[2], Annalisa Del Prete[1], Paramahamsa Maturu[1], John O. Trent[1,3], and Bodduluri Haribabu[1,2]

[1]Tumor Immunobiology Program, James Graham Brown Cancer Center and [2]Departments of Microbiology and Immunology, [3]Medicine, University of Louisville Health Sciences, Louisville, KY 40202.

Running Title: LTB_4 Binding Site and Activation of BLT1

Author(s) for correspondence: Bodduluri Haribabu, Ph.D., The James Graham Brown Cancer Center, University of Louisville, 580-South Preston Street, Louisville, KY-40202; Tel.: 502 852-7503, Fax: 502 852 2123 E-mail H0bodd01@gwise.louisville.edu
or John O. Trent, Ph.D., The James Graham Brown Cancer Center, University of Louisville, 529 South Jackson Street, Louisville, KY-40202; Tel.: 502 852-2194, Fax: 502 852 4311
E-mail john.trent@louisville.edu

Leukotriene B_4 mediates a variety of inflammatory diseases such as asthma, arthritis, atherosclerosis and cancer through activation of the G-protein coupled receptor, BLT1. Using *in silico* molecular dynamics simulations combined with site directed mutagenesis we characterized the ligand binding site and activation mechanism for BLT1. Mutation of residues predicted as potential ligand contact points in transmembrane domains (TMs) III (H94, Y102A), V (E185A) and VI (N241A) resulted in reduced binding affinity. Analysis of arginines in extracellular loop 2 (ECL2) revealed that mutating arginine 156 but not arginine 171 or 178 to alanine resulted in complete loss of LTB_4 binding to BLT1. Structural models for the ligand-free and ligand-bound states of BLT1 revealed an activation core formed around D64, displaying multiple dynamic interactions with N36, S100, N281 and a triad of serines, S276, S277 and S278. Mutagenesis of many of these residues in BLT1 resulted in loss of signaling capacity while retaining normal LTB_4 binding function. Thus, polar residues within TMs III, V and VI and ECL2 are critical for ligand-binding while polar residues in TMs II, III and VII play a central role in transducing the ligand-induced conformational change to activation. The delineation of a validated binding site and activation mechanism should facilitate structure-based design of inhibitors targeting BLT1.

Seven transmembrane receptors widely known as G-protein coupled receptors (GPCRs) (1,2) mediate an array of physiological processes in response to such diverse agonists as peptides, amino acid derivatives and lipids. Despite the great diversity in their ligands, the conserved motifs found across this super family and the limited interacting partners such as G-proteins (3) and β-arrestins (4) at the cytoplasmic interface point towards a common activation mechanism for GPCRs. GPCRs constitute the single largest group of molecules for drug targets due to their critical importance in mediating biological responses as well as their easy accessibility on the cell surface. However, very little structural information is available for GPCRs due to difficulties in purifying and obtaining crystal structures for this class of receptors.

The availability of the rhodopsin crystal structure (5) combined with the approach of computational modeling and validation by site-directed mutagenesis has led to delineation of ligand-receptor interactions in a few GPCRs (6-9). Some elements of the activation mechanism have been identified for individual GPCRs (1,6,8,10-12). Several studies employing site directed mutagenesis have helped uncover critical interactions between residues in transmembrane domains of the GPCRs (reviewed in (1)). The approach of computational modeling with validation by site-directed mutagenesis has led to significant

increases in the understanding of the processes involved in GPCR activation (6-9).

Leukotriene B_4 (LTB_4) is a potent leukocyte chemoattractant and mediates its biological effects through two distinct G-protein coupled receptors, the high affinity receptor BLT1 and the low affinity receptor BLT2 (13,14). Several recent studies suggested a direct and critical role for BLT1 in diverse inflammatory diseases such as arthritis (15,16), atherosclerosis (17,18) and asthma (19). Recently, the high affinity LTB_4 receptor, BLT1 was expressed in *E.coli* and shown to form a functional pentameric complex with hetero-trimeric G-proteins (20). Computational modeling has been used to investigate the potential role of the eighth helix in signaling of BLT1 (21,22). In addition, a recent study reported an LTB_4 binding site in BLT1 deduced from computational models (23). However, the exact nature of the LTB_4 binding site and the potential changes in receptor conformation following LTB_4 binding remain unknown.

In this study, computational modeling together with site-directed mutagenesis led to precise mapping and validation of the LTB_4-binding site in BLT1. Mutation of each of the residues predicted to be in the putative binding site resulted in reduced binding affinity. Furthermore, analysis of dynamic structures of the ligand-free and ligand-bound BLT1 allowed prediction of critical movements of transmembrane helices and essential inter-helical interactions stabilizing both the active and inactive states of the receptor. This analysis uncovered an activation core centered around D64 (D2.50-Ballesteros-Weinstein numbering system) (11) and comprised of polar amino acids N36 (N1.50), S100 (S3.35), S277 (S7.45), S278 (S7.46), S279 (S7.47) and N281 (N7.49) and led to the formulation of an activation mechanism. The deduced mechanism of BLT1 activation was consistent with the experimental observations made with several mutants of activation core residues.

Experimental Procedures

Homology modeling and identification of LTB_4 binding site in BLT1: The multiple alignment of the human LTB_4 receptors, BLT1 and BLT2, with bovine rhodopsin was generated using CLUSTALW (24). The alignment was in agreement with known literature on helix stabilization motifs, disulphide linkage conservation and core forming residue conservation in GPCRs (25) and was used to generate homology models based on the crystal structure of Bovine Rhodopsin (5) (PDB id; 1F88.ent) as a template in Modeler (26). The homology model of BLT1 was energy minimized (hydrogen atom addition by xleap and minimized using 5000 steps of steepest descent followed by 20,000 steps of conjugate gradient using AMBER8 (27) sander with ff99) and then used for docking with LTB_4. A structure for LTB_4 was generated in SYBYL7.0 (SYBYL 7.0, Tripos Inc., 1699 South Hanley Rd., St. Louis, Missouri, 63144, USA) and charges and potentials were assigned to the receptor (Kollman All) and ligand (gasteiger). A consensus docking approach was used wherein multiple docking algorithms were employed to improve the scoring process. LTB_4 was docked into BLT1 using, DOCK (28), SURFLEX (29) and AUTODOCK (30). The consensus structure for ligand docked BLT1 was refined using restricted molecular dynamics using the SYBYL7.0 dynamics module, employing the AMBER 7 FF99 for 500ps with a 1fs time step. The "aggregates" option was employed to keep frozen (fixed) all the parts of the receptor except the ligand and the ligand binding pocket as defined by a radius of 8Å with the ligand as center. The resulting structure was then energy minimized (5000 steps of steepest descent followed by 20,000 steps of conjugate gradient) and molecular dynamics simulations *in vacuo*, were carried out (100K, 25ps followed by 300 K for 125 ps with positional restraints of 1000 kcal (mol $Å)^{-1}$) using AMBER8 (27) (sander ff99) on the entire receptor excluding the above defined binding pocket residues and the ligand, which were left unrestrained to further optimize contacts and relax the pocket. The binding mode was visualized using Insight II (Accelrys Inc) and SYBYL7.0. Figures were generated with Insight II, Molscript (31) and Raster3D (31).

Molecular Dynamics Simulations: Molecular dynamics simulations of the ligand-bound and ligand-free forms of the receptor were carried out in a lipid bilayer solvated system consisting of lipid, water and ions using previously reported protocols (32). Specifically, xleap was used to generate the solvated lipid bilayer system, comprised of the homology model of BLT1, 375 pre-equilibrated dodecyl maltoside lipid molecules, 10111 TIP3P solvent molecules and Cl^- ions added for neutrality. Our standard equilibrium and production run protocols were used (32). Molecular dynamics simulations were performed using the AMBER-99 force field using AMBER 8.0. and the mpi Sander module in the isothermal isobaric ensemble (p=1 atmosphere) and anisotropic pressure scaling (ntp=2); periodic boundary conditions with PME; 1.5 fs time step; hydrogen atoms frozen using SHAKE. The ligand was parameterized with antechamber program (33) using the GAFF (general amber force field) and HF/6-31G* derived RESP atomic charges from GAMESS. The production runs were unrestrained and run for 5 ns using 32 Opteron processors. The same protocol was followed for both BLT1 with and without the bound natural agonist, LTB_4.

Molecular dynamics trajectories were analyzed via Energy *versus* Time and Root Mean Square Deviation (RMSD of backbone atoms) *versus* Time for the post equilibration production phase. The analysis established the energetic and structural stability of the system for both ligand-free and ligand-bound BLT1 simulations.

Site directed mutagenesis: The construction of cDNA of hemagluttinin (HA) epitope tagged BLT1 was described previously (34). A Red Fluorescent Protein-Monomer (RFP-Mono) was tagged at the C-terminus of BLT1 by in frame cloning the entire coding region of the receptor without a stop codon ahead of the RFP-coding region in pDsRed-Monomer N1 vector (BD biosciences # 632465). Site specific mutants of BLT1-RFP-Mono were generated using the PCR based sense-anti sense primer method (35) and all mutants were confirmed by DNA sequencing.

Expression of receptors and generation of clonal stable cell lines: Functional properties of the native and mutant receptors were examined in 300.19 cells. 300.19 is a murine pre-B cell line with no detectable endogenous expression of any LTB_4 responsive receptors and was previously used to study the signal transduction pathways activated by leukocyte adhesion molecules (36) and chemokine receptors (37). 300.19 cells were maintained in RPMI supplemented with 10% FBS, 100 U/ml penicillin, 100 μg/ml streptomycin and 55 μM 2-mercaptoethanol and transfected by electroporation. The stable single cell derived cell lines with BLT1 or its mutants were selected by FACS (Moflo) and maintained in the presence of 1 mg/ml of G418. The cell surface expression was determined by incubating parental cells or cells expressing different receptor variants with 12CA5 antibody followed by FITC-labeled goat anti-mouse IgG and analyzed using BD FACScalibur.

Ligand binding: Whole cell competition ligand binding (34) or saturation binding (13) assays were performed with 300.19 cells expressing BLT1 or its mutants. For competition binding assay, the cells (0.5×10^6 per assay) were incubated with 2.5 nM ^{3}[H] LTB_4 (0.25 nM for BLT1) (163 Ci/mmol; Perkin Elmer, Boston, MA) along with increasing concentrations of cold ligand (Cayman chemicals, Detroit, MI) in binding buffer (50 mM Tris-HCl pH 7.4, 10 mM $MgCl_2$, 10 mM NaCl, 0.05% BSA (Fatty acid free Fraction V, Sigma # A8806)). These mixtures were incubated on ice with gentle agitation for 2 h followed by rapid filtration through GF/C filters (Whatman #1822-025) using Manifold-Vacuum setup and washed with 3 ml of ice cold binding buffer. The radioactivity of the filters was determined with Beckman Coulter LS6500 Multi Purpose Scintillation Counter. Nonspecific binding was determined by inclusion of 2 μM unlabeled LTB_4 to the cells suspended in 2.5 nM ^{3}[H] LTB_4. The competition curves were generated using Non-linear regression fit on Graphpad PRISM software and the EC50 determined.

Saturation binding was also performed using whole cells. The binding mixture contained whole cells and ^{3}H–LTB_4 at various concentrations with or without unlabeled LTB_4 in 1,000 fold excess. The 100 μL binding reactions were incubated at 4 °C for two hours followed by rapid filtration through GF/C filters and radioactivity was measured as described above. The saturation binding curves were generated using one site binding (hyperbola) non-linear regression curve fitting (Graphpad PRISM 4.0). K_d and B_{max} were determined from these curves and expressed as nM and binding sites/cell, respectively. Similar values were obtained from Scatchard analysis of the data.

Chemotaxis and calcium measurements: Migration of 300.19 cells was evaluated using 5-μm pore size Transwell filters (Corning Costar, Cambridge, MA). Cells (1x 10^7) were resuspended in 1 ml of chemotaxis buffer (RPMI-1640, 1% FBS). The lower chamber was loaded with various concentrations of LTB_4 in a volume of 600 μL and 100 μL (1x10^6 cells) of cells from above cell suspension was placed onto the upper chamber. After 3 h of incubation at 37 °C in 5% CO_2, the upper chamber was removed and cells in the lower chamber were counted in a Bürker chamber. Calcium mobilization was monitored in INDO-I loaded cells (300.19 cells expressing BLT1-WT or its mutants) stimulated with various concentrations of LTB_4 as previously described (34).

Receptor phosphorylation: 300.19 cells (5 million cells per sample) expressing BLT1-RFP or its mutants were serum-starved for 2 h in 5 ml phosphate-free DMEM medium with 20 mM HEPES, pH 7.0. Cells were washed with the same buffer and labeled with ^{32}P-orthophosphate (150 μCi per sample; 8500-9120 Ci/mmol, Perkin Elmer, Boston, MA) in above buffer in the total volume of 1.5 ml for 1.5 hrs and cells were stimulated for 5 min at 37 °C with LTB_4 at indicated concentrations. Cells were washed twice with ice cold 1X PBS (w/o Ca^{2+} and Mg^{2+}) containing 0.1% BSA. The harvested cells were lysed with 1 ml of RIPA Buffer (50 mM Tris-Cl (pH 8), 150 mM NaCl, 1% NP-40, 0.5% deoxycholate, 0.1% SDS, 1 mM EDTA, 1 mM NaF, 1 mM Sodium pyrophosphate and protease cocktail inhibitor tablet from Roche). HA-tagged receptors were immuno-precipitated with high affinity anti-HA antibody (clone 3F10 from Roche). Immunoprecipitates were resolved by 10% SDS-PAGE and dried gels were exposed to phosphor imager screens and analyzed on Typhoon 9400 (Amersham BioSciences). Integrated counts were evaluated using ImageQuant software (Amersham Biosciences).

Real-time Fluorescence Microscopy: RBL-2H3 cells were co-transfected with β-arrestin-GFP and either with wild type or mutant receptor tagged with RFP (Mono) and images were captured as described (18,34).

Results

Identification of LTB_4 binding site in BLT1: Bovine rhodopsin had been the only available crystal structure (5) for a GPCR and hence heavily relied upon for homology modeling based approaches for structural studies of GPCRs. The rhodopsin ligand (11-cis retinal) is covalently linked to the receptor whereas LTB_4 is a mostly hydrophobic lipid with three nodes of polarity. The polar head group is a carboxylate which can form hydrogen bonding or strong ionic interactions, and the hydroxyl groups at the 5^{th} and 12^{th} carbon positions are also capable of forming hydrogen bonding interactions.

To obtain a starting structure for BLT1, a sequence alignment of human BLT1 with bovine rhodopsin (1F88) was generated. This alignment was then manually modified to precisely match the known motifs in the transmembrane (TM) regions for rhodopsin with those of BLT1. A homology-based 3-dimensional structural model for the human BLT1 that included a conserved disulphide linkage between Cys90-Cys168 (25,38) was generated and energy minimized.

A “consensus docking protocol” that used three independent docking algorithms: AUTODOCK (30), SURFLEX (29) and DOCK (28), was employed to obtain a ligand-docked structure for BLT1. The top three

ranked results from each of the docking runs were analyzed, and the highest common factor or the most common binding mode was selected as a starting binding mode for LTB_4 in BLT1. This structure of LTB_4 docked into BLT1 was subjected to minimization and *in vacuo* molecular dynamics allowing both the receptor binding pocket and the ligand to relax and attain stable conformations of lowest energies. A snake diagram depicting the primary sequence of BLT1 is shown in Fig 1A. The residues identified as ligand contact points are marked in green. The structure of LTB_4 bound to BLT1 is shown in (Fig. 1B). The ligand-binding site of BLT1 is composed of ECL2, TMs III, V and VI and the hydrophobic ligand penetrates deep into the transmembrane domains. The three nodes of polar-regions in the ligand are countered by corresponding polar residues in the receptor. A clear ligand-binding pocket is visible in the surface rendering of the LTB_4 binding site of BLT1 (Fig. 1C).

LTB_4 interaction with residues in transmembrane domains: The hydrophobic nature of the ligand suggested a deep seated pocket within BLT1. Analysis of the ligand bound structure identified several potential contact points in the TMs: H94 and Y102 (TM III), E185 (TM V) and N241 (TM VI) while the polar head group was oriented towards ECL2 (Fig. 2A). Both E185 (TM V) and Y102 (TM III) stabilize LTB_4 binding by direct hydrogen bonding with the C5' hydroxyl group as well as with each other whereas N241 (TM VI) hydrogen bonds to the hydroxyl group on C12' of LTB_4 at the base of the binding pocket. H94 likely interacts with the C5'-hydroxyl of LTB_4 via hydrogen bonding.

To validate these interactions, receptor variants were generated by mutagenesis. Amino acid residues H94, Y102, N241 and E185 were mutated to alanine in a combination of single and double mutants. All these receptor variants were stably expressed to similar levels as single cell derived lines on the surface of 300.19 cells (Fig. 2B). All the mutants displayed reduced levels of binding as determined by both competition and saturation binding assays (Fig. 2C, D, E and Table 1). The four single mutants H94A, Y102A, N241A, and E185A displayed reduced binding affinity of 4 to 9 fold in competition binding and 6 to 15 fold in saturation binding assays (Table 1). Surface expression as measured by flow cytometry or as B_{max} in saturation binding assays also showed that all mutants are expressed at comparable or higher levels relative to BLT1 (Table 1). The Y102A/N241A double mutant showed a synergistic reduction in binding affinity in ^{3}H-LTB_4 binding assays (Fig. 2E and Table 1). LTB_4 activates a variety of cellular responses including chemotaxis (14), calcium mobilization, ligand-induced phosphorylation and desensitization (39). Consistent with the reduction in binding, all the mutants showed a shift in dose response of chemotaxis (Fig. 2F) while retaining the bell-shaped nature of the response. The Y102A/N241A double mutant required 100 times more LTB_4 for reaching the maximum response. Analysis of ligand-induced calcium mobilization also showed a clear shift in dose response with each of these mutants (Fig. 3). The Y102A, H94A, N241A and the Y102A/N241A double mutants reached similar levels of maximum activity but at much higher concentrations than the wild type receptor (Fig. 3). A summary of the functional properties of all the mutants is shown in (Table 1).

***A Critical role for ECL2 in LTB_4 binding*:** The ligand-docked structural model showed R156 and T157 being located on ECL2 which caps the binding site on top of the TM helix bundle. A charge interaction between R156 and the carboxylate group of LTB_4 was predicted to stabilize LTB_4 in the binding pocket. The model also predicted T157 as being within hydrogen bonding distance of the carboxylate head group of LTB_4. The other possible charge interactions on ECL2 were with R171 and R178.

In order to delineate the relative contribution of these residues to ligand binding, the R156A/T157A (RT/AA), R171A/R178A (RR/AA), R156A and T157A mutants were stably expressed to similar levels in 300.19 cells (Table 1). The R156A/T157A and the R156A mutants failed to show any [^{3}H]-LTB_4 binding, whereas the

T157A and R171A/R178A mutants displayed similar ligand binding affinity as BLT1 (Table 1). Consistent with the complete lack of LTB_4 binding the R156A/T157A and R156A mutants did not show a detectable chemotactic response (Fig 4A). In contrast, both the T157A and R171A/R178A mutants showed a similar bell shaped chemotaxis response as BLT1 (Fig 4A). Likewise, ligand-induced calcium mobilization by all these mutants followed a similar profile with R156A/T157A and the R156A mutants showing a minimal response and T157A and R171A/R178A showing a similar response as BLT1. Thus, R156 is a critical residue for LTB_4 binding, and as a consequence, for signaling in BLT1.

Ligand-Induced phosphorylation of BLT1 mutants: Concomitant with activation, ligand binding induces a dose-dependent phosphorylation of the GPCRs by G-protein coupled receptor kinases (GRKs) (40) leading to desensitization of signaling. Previous studies have shown that BLT1 displays a basal level of phosphorylation that is enhanced by treatment with LTB_4 (34). (Fig. 5) shows that BLT1 undergoes rapid LTB_4 dose-dependent phosphorylation and all the binding site mutants also displayed ligand-induced phosphorylation but required higher LTB_4 concentrations to be fully phosphorylated. The RT mutant while displaying basal phosphorylation did not show any further increase in receptor phosphorylation at any concentration of LTB_4.

Inactive and Active States of BLT1: An experimentally validated ligand binding mode in BLT1 described above formed the basis to examine the ligand-induced conformational changes in BLT1. Lipid bilayer molecular dynamics simulations were run for the ligand-free and ligand-docked homology modeled structures of BLT1 to generate optimized inactive and active state models. A comparison of the models of the ligand-free and ligand-bound states of BLT1 by superimposition revealed movement of transmembrane helices (Fig. 6A and 6B) as well as conformational changes at the amino acid level (see below). TMs I, II and IV show minimal movement, TMs III and V show moderate movement, and TMs VI and VII show the largest transmembrane helical movement (Fig 6A and 6B). The large conformational changes observed in TMs VI and VII of BLT1 are consistent with similar changes associated with the activation of rhodopsin (41-43).

Identification of an Activation Core in BLT1: Hydrogen bonding, Van der Waals and electrostatic interactions were analyzed for both the inactive and active states of BLT1. A cluster of polar residues comprised of N36, D64, S100, N281, S277, S278 and S279 were found to differentially stabilize the inactive and active states of BLT1 and form the activation core. (Fig. 7A & 7B) Both, in the inactive (Fig. 7A) and active states (Fig. 7B), D64 was the hub of the interactions. In the inactive state, D64 was hydrogen bound with S100 (d = 2.6Å) and S278 (d = 2.7Å). The S100-D64 and S278-D64 interactions were conserved in both the inactive and active states of BLT1 (Fig. 7A and 7B). During activation, N281 and N36 moved upwards by 3.2Å and 7Å (Fig 7B) respectively to hydrogen bond with D64. These interactions are completely absent in the inactive state (Fig 7A).

To determine the validity of this activation mechanism each of these polar residues were mutated to alanine and the mutant receptors were stably expressed to similar levels in clonal lines of 300.19 cells (Fig. 7C and Table 2). All of these mutants displayed ligand-binding affinity similar to the wild type BLT1 both in competition and saturation binding assays (Table 2) with the exception of the S277-79A mutant that bound LTB_4 with reduced affinity (Table 2). Saturation binding analysis also showed that each of the mutants is expressed at similar or higher levels relative to BLT1 (Table 2).

Analysis of the activation core mutants for chemotaxis, calcium mobilization, ligand-induced phosphorylation, β-arrestin association and internalization revealed severe reduction in their activity relative to BLT1. First, all mutants displayed reduced chemotaxis with N281A showing a complete loss of response (Fig. 7D). D64A and S277-79A showed a shift as well as a reduction in response. Despite the significant reduction in

magnitude, all mutants showed a bell shaped chemotaxis curve indicating normal gradient sensing by these mutants.

Dose dependent calcium mobilization also showed a severe reduction in response for many of these mutants (Fig 8A-D). While the maximum response reached for the D64A mutant was only ~25% that of the BLT1 response, other mutants reached 60 to 100% response to that of native BLT1. However, much greater inhibition was seen at the EC90 of the BLT1 response, where for most mutants the response ranged from 0 to 10%. In particular, the D64A and N281A mutants showed very little response at 1.0 and 10 nM LTB_4 (Fig. 8 B and C, Table 2). Thus, despite similar binding affinity for LTB_4, these BLT1 mutants fail to convert ligand binding into an effective cytoplasmic signal. Simultaneous with receptor activation, ligand binding affects a dose dependent phosphorylation of GPCRs by G protein coupled receptor kinases (GRKs) (40) leading to desensitization as well as association of the phosphorylated receptors with β-arrestin. BLT1 and all the activation core mutants showed a basal level of receptor phosphorylation as well as a comparable increase in PMA-induced phosphorylation (44) (Fig. 8E and 8F). While BLT1 showed a robust increase in ligand-induced phosphorylation, most activation core mutants displayed relatively weak ligand-induced phosphorylation (Fig. 8E and 8F). Consistent with the complete loss of chemotaxis response and severe reduction in calcium mobilization, the N281A mutant showed no ligand-induced phosphorylation but was a substrate for PMA-induced phosphorylation. Translocation of cytoplasmic β-arrestin to the membrane is a ubiquitous phenomenon following GPCR activation (45). (Fig 8G) shows the typical rapid β-arrestin translocation following LTB_4 treatment of cells expressing BLT1-RFP and β-arrestin-GFP. In this assay N281A failed to interact with arrestin, whereas the other mutants displayed relatively weak or delayed association of β-arrestin with RFP-receptors (Fig. 8G). Thus, despite similar binding affinity for LTB_4, these BLT1 mutants fail to convert ligand binding into an effective cytoplasmic signal.

Discussion

Computational models identified the potential contact points for LTB_4 in BLT1 that were validated by mutational analysis. Molecular dynamics analysis of the ligand-free and ligand-bound structural models of BLT1 predicted essential residues involved in differentially stabilizing the inactive and active states of the receptor via critical polar interactions. Experimentally, these were proven to affect the signaling mechanism supporting a conceptual activation core in class A GPCRs. A high degree of conservation of the polar activation core residues across the class A GPCRs lends further support for the mechanism.

The use of multiple docking protocols and molecular dynamics of the binding pocket allowed the delineation of the LTB_4 binding site in BLT1. Experimental results with mutants support the accuracy of the predicted binding mode, validating this approach. The hydrophobic nature of LTB_4 dictates to a large extent it's deep seated binding mode in the BLT1 pocket. The ligand is encompassed by transmembrane domains III, V and VI, while ECL2 forms a lid over the pocket. Each of the three TM's contribute residues towards ligand binding (H94 and Y102 in TM-III, E185 in TM-V and N241 in TM-VI). The three nodes of polarity in LTB_4 are being countered by four polar residues in the receptor and mutation of each had a measurable effect on binding affinity and signaling. The N241A, Y102A, E185A, H94A and the Y102A-N241A double mutant, each attained the wild type maximum levels of signaling in functional assays including chemotaxis, calcium flux and receptor phosphorylation, albeit at a much higher concentration of LTB_4 as compared to BLT1. This suggests that while these residues located in TMs III, V and VI contribute to the binding affinity by countering the hydroxyl groups at 5^{th} and 12^{th} positions on LTB_4, they are not absolutely critical for LTB_4 binding or ligand–induced conformational changes associated with receptor activation. In contrast, interaction of the carboxylate head group with ECL2 is absolutely critical for binding. While both R156 and T157 were predicted to be involved

in ligand binding, analysis of double and single mutants established the critical role of R156 in LTB_4 binding. Mutation of arginine 156 to alanine resulted in minimal levels of signaling as expected from the complete loss of ligand binding. These findings suggest a more critical role for ECL2 residues in LTB_4 binding than that for the transmembrane domains. The negative charge of the carboxylate head group of LTB_4 is effectively countered by the positively charged arginine residue (R156). The ECL2 may be involved in initial ligand entry as well as being critical for ligand stabilization via a hinged lid-like action closing and completing the binding pocket. An integral role for ECL2 in ligand binding has also been reported for other GPCRs (46,47).

A recent study reported a molecular modeling based binding pocket for LTB_4 in BLT1 (23). The study concludes with the identification of Arg178 and Glu185 as residues involved in ligand receptor interactions and Val 105 and Ile 108 as lining the binding pocket. In general, the overall binding modes described here and in Sabirsh et al. (23) are similar in that the orientation of the ligand along the receptor axis, with the hydrophobic tail seated deep in the core and the polar head group pointing towards the extracellular surface. Secondly, the E185 was identified as a ligand binding residue by both models via interaction with the C5'hydroxyl group of LTB_4.

However, the binding mode proposed here differs from Sabirsh et al. with respect to identification of the residues involved in ligand stabilization, the magnitude of the effects of point mutations on ligand binding and the experimental and computational strategies employed to arrive at these conclusions. The studies here identify and validate H94, Y102, N241 and R156 as residues involved in LTB_4 binding to BLT1 while none of these residues were considered by Sabirsh et al. (23). In contrast, they have indicated R178 as a binding site residue based on the R178L mutation. The magnitude of the effect on ligand binding observed in Sabirsh et al. upon mutating Arg178 to Leu could possibly be a result of the energetic penalty arising out of replacing a polar residue by a highly hydrophobic residue. In our study, mutating R178 to alanine had no effect on ligand binding. In contrast, it is the R156 on ECL2 that is most critical for LTB_4 binding as evidenced by complete loss of binding in the R156A mutant while being expressed normally on the cell surface. Alanine substitution was used as a mutagenesis strategy for all our analysis as this would minimize other indirect effects.

The differences in the structural models may be accounted for by the contrasting computational strategies employed. While Sabirsh et al. based their model of BLT1 on a theoretical active state model of rhodopsin; our models were based on the crystal structure of inactive state bovine rhodopsin (PDB id: 1F88.ent). In our studies, LTB_4 was successfully docked into the inactive state of BLT1 in a minimum energy conformation following a consensus docking approach. It is important to note that docking LTB_4 into a lipid bilayer simulated structure of BLT1 in it self was insufficient to accurately identify all the interactions. Further, the use of fully solvated lipid bilayer molecular dynamics simulations might better approximate the receptor microenvironment as compared to energy minimized homology models developed by Sabirsh et al. (23).

A few of the residues identified in this study as being critical to LTB_4 binding in BLT1 have been implicated in mediating ligand binding via congruent positions in other class A GPCRs. The E185 residue in BLT1 finds a parallel in the E182 residue of the histamine binding site of the histamine H4 receptor (48). Similarly, an equivalent of the H94 residue (TM III) has been shown to play a critical role in ligand recognition in the human A3 adenosine receptor as H95 (49). The fMLP binding site in its receptor was dissected using a chimeric approach and revealed the essential role of extracellular loops in ligand binding (50). An essential role for R156 (ECL2) in ligand binding in BLT1 was established in this study. Interestingly, arginines in ECL2 were shown to be important in ligand binding in several other chemoattractant receptors. In prostaglandin D_2 receptor (CRTH2) R178A mutation in ECL2 resulted in a five fold decrease in the binding affinity (51). In CCR5,

R168 in ECL2 is essential for binding MIP1 alpha (52). Similarly, it has been shown in the C5a receptor that arginine 175 is an important counter-ion in binding C5a. In CXCR3, arginine 197 and arginine 212 in ECL2 are critical for ligand binding whereas arginine 216 is critical for receptor activation but not for ligand binding or internalization (53). Given the chemical diversity of the GPCR ligands, these examples highlight the role of arginines in ECL2 in ligand binding in GPCRs.

The residues Y102, R156, E185 and N241 are all conserved in the low affinity LTB_4 receptor BLT2 but the H94 is replaced by Y in BLT2. Despite the limited homology between BLT1 and BLT2 (~45%), conservation of most of the binding site residues described here suggests a common binding mode for LTB_4 in BLT1 and BLT2. The difference in the binding affinities between BLT1 and BLT2 for LTB_4 may thus be related to the replacement of H94 with Y and other possible changes in helical orientation and/or interaction distances between the key binding residues in BLT2. Application of similar strategies described here should allow precise identification and rationalization of LTB_4 binding site in BLT2. The elucidation of the LTB_4 binding site renders BLT1 amenable to structure based drug design.

The BLT1 structures with and without bound LTB_4 allowed delineation of the ligand-induced conformational changes leading to a preliminary activation mechanism. In the generalized toggle switch activation mechanism (54) of GPCRs, TM VI (55) and VII (42) are known to move outwards at the extracellular face of the receptor. Similar helical movements were observed for BLT1 activation, and the final alignment of TM VI and VII were consistent to both in rhodopsin (12,41,55) and in the generalized toggle switch mechanism. Upward and downward movements of the helices resulted in an increased cytoplasmic penetration of ICL's 2 and 3 in the active state of the receptor. This, along with a more open arrangement of the TMs at the cytoplasmic face, is consistent with the need for increased surface area for interaction with signaling partners such as G-proteins and β-arrestin. The model for BLT1 is also consistent with respect to only minimal changes being seen for TMs I through IV (54).

A unique element of the current study is that molecular dynamic simulations were predictive and allowed rationalization of global changes in receptor conformation to altered interactions at the level of a few amino acid residues. These residues couple the ligand-binding domain to signaling via appropriate conformational changes. The receptor variants generated by site-directed mutagenesis of the activation core residues allowed uncoupling of ligand binding function from signaling function. Both D64A and N281A mutants bind LTB_4 with the same affinity as BLT1 yet activate minimal signaling functions. Thus, reorientation of helix VII bringing the N281 in juxtaposition to D64 appears a critical event for stabilizing the active state of BLT1. The D64-N281 interaction has been implicated as being critical in several other GPCRs.(1,6,8) An interesting difference in the GnRH (56) receptor is D64 and N281 are replaced by N87 and D318. The residues when reversed at this position retained wild type receptor functions, whereas single mutants were defective in ligand binding. In the case of the serine triad S277-79 the interactions were more complex, as W234 stabilizes the inactive state via hydrogen bonds with S278 but switches to S277 in the active state. In the serine triad mutant loss of stabilizing forces both in the active and inactive states of the receptor might have resulted in the observed phenotype of both reduced binding affinity as well as signaling capacity.

The general applicability of the proposed BLT1 mechanism to other class A GPCRs was examined in 1636 sequences from the GPCR data base (www.gpcr.org). The activation core residues at positions N36, D64, S100, S277, S278, S279, and N281 occur at a frequency of N36 (100 %), D64 (91.25%), S100 (<1%), S277 (13.5%), S278 (29.9%), S279 (6.8%) and N281 (64%). At the "SSS" locus, depending on the receptor subclass there exist other common motifs for GPCRs such as HCC, NSC, NSS and other such combinations

of polar residues. Of the 1636 GPCRs analyzed nearly 100% have conserved polar residues at positions equivalent to N36 and D64, while other positions also showed high levels of polar residue conservation across class A GPCRs (Table-3). Thus, at congruent positions to those identified in BLT1, conservation of polarity rather than exact identity of the residues might be critical for GPCR function (57,58). It is possible that each of these conserved positions in other GPCRs represent similar elements of the activation mechanism as seen for BLT1.

The polar residues comprising the ligand binding site and activation core are critical in coupling LTB_4 binding to signaling in BLT1. Further studies will establish the significance of hydrophobic residues in receptor function.

Acknowledgements: This work was supported by the NIH grant AI52381 to BH and SB was supported by an American Heart Association Pre-doctoral award.

Abbreviations: GPCR: G-Protein coupled receptors, ECL: Extracellular loop, ICL: intracellular loop, BLT1: Leukotriene B_4 Receptor-1, BLT2: Leukotriene B_4 Receptor-2 LTB_4: Leukotriene B_4, TM: Transmembrane, MD: Molecular dynamics, FF- Force field, PS: Pico seconds, NS: Nano seconds, RFP: Red fluorescence protein, GFP: Green fluorescence protein, FITC: Fluorescein Isothiocyanate, HA: Hemagglutinin Antigen, FBS: Fetal bovine serum, EC50: Effective concentration 50, BSA: Bovine serum albumin, SDS-PAGE: Sodium Dodecyl Sulfate Polyacrylamide Gel Electrophoresis, GRK: G-protein coupled receptor kinase.

References

1. Kristiansen, K. (2004) *Pharmacol Ther* **103**, 21-80
2. Gether, U. (2000) *Endocr Rev* **21**, 90-113
3. Cabrera-Vera, T. M., Vanhauwe, J., Thomas, T. O., Medkova, M., Preininger, A., Mazzoni, M. R., and Hamm, H. E. (2003) *Endocr Rev* **24**, 765-781
4. Lefkowitz, R. J., and Shenoy, S. K. (2005) *Science* **308**, 512-517
5. Palczewski, K., Kumasaka, T., Hori, T., Behnke, C. A., Motoshima, H., Fox, B. A., Le Trong, I., Teller, D. C., Okada, T., Stenkamp, R. E., Yamamoto, M., and Miyano, M. (2000) *Science* **289**, 739-745
6. Urizar, E., Claeysen, S., Deupi, X., Govaerts, C., Costagliola, S., Vassart, G., and Pardo, L. (2005) *J Biol Chem* **280**, 17135-17141
7. Fanelli, F., and De Benedetti, P. G. (2005) *Chem Rev* **105**, 3297-3351
8. Jongejan, A., Bruysters, M., Ballesteros, J. A., Haaksma, E., Bakker, R. A., Pardo, L., and Leurs, R. (2005) *Nat Chem Biol* **1**, 98-103
9. Spijker, P., Vaidehi, N., Freddolino, P. L., Hilbers, P. A., and Goddard, W. A., 3rd. (2006) *Proc Natl Acad Sci U S A* **103**, 4882-4887
10. Decaillot, F. M., Befort, K., Filliol, D., Yue, S., Walker, P., and Kieffer, B. L. (2003) *Nat Struct Biol* **10**, 629-636
11. Sealfon, S. C., Chi, L., Ebersole, B. J., Rodic, V., Zhang, D., Ballesteros, J. A., and Weinstein, H. (1995) *J Biol Chem* **270**, 16683-16688
12. Sakmar, T. P., Menon, S. T., Marin, E. P., and Awad, E. S. (2002) *Annu Rev Biophys Biomol Struct* **31**, 443-484
13. Yokomizo, T., Kato, K., Terawaki, K., Izumi, T., and Shimizu, T. (2000) *J Exp Med* **192**, 421-432
14. Yokomizo, T., Izumi, T., Chang, K., Takuwa, Y., and Shimizu, T. (1997) *Nature* **387**, 620-624
15. Kim, N. D., Chou, R. C., Seung, E., Tager, A. M., and Luster, A. D. (2006) *J Exp Med* **203**, 829-835

16. Shao, W. H., Del Prete, A., Bock, C. B., and Haribabu, B. (2006) *J Immunol* **176**, 6254-6261
17. Helgadottir, A., Manolescu, A., Helgason, A., Thorleifsson, G., Thorsteinsdottir, U., Gudbjartsson, D. F., Gretarsdottir, S., Magnusson, K. P., Gudmundsson, G., Hicks, A., Jonsson, T., Grant, S. F., Sainz, J., O'Brien, S. J., Sveinbjornsdottir, S., Valdimarsson, E. M., Matthiasson, S. E., Levey, A. I., Abramson, J. L., Reilly, M. P., Vaccarino, V., Wolfe, M. L., Gudnason, V., Quyyumi, A. A., Topol, E. J., Rader, D. J., Thorgeirsson, G., Gulcher, J. R., Hakonarson, H., Kong, A., and Stefansson, K. (2006) *Nat Genet* **38**, 68-74
18. Jala, V. R., and Haribabu, B. (2004) *Trends in Immunology* **25**, 315-322
19. Miyahara, N., Takeda, K., Miyahara, S., Matsubara, S., Koya, T., Joetham, A., Krishnan, E., Dakhama, A., Haribabu, B., and Gelfand, E. W. (2005) *Am J Respir Crit Care Med* **172**, 161-167
20. Baneres, J. L., and Parello, J. (2003) *J Mol Biol* **329**, 815-829
21. Okuno, T., Ago, H., Terawaki, K., Miyano, M., Shimizu, T., and Yokomizo, T. (2003) *J Biol Chem* **278**, 41500-41509
22. Okuno, T., Yokomizo, T., Hori, T., Miyano, M., and Shimizu, T. (2005) *J Biol Chem* **280**, 32049-32052
23. Sabirsh, A., Bywater, R. P., Bristulf, J., Owman, C., and Haeggstrom, J. Z. (2006) *Biochemistry* **45**, 5733-5744
24. Eddy, S. R. (1995) *Proc Int Conf Intell Syst Mol Biol* **3**, 114-120
25. Rader, A. J., Anderson, G., Isin, B., Khorana, H. G., Bahar, I., and Klein-Seetharaman, J. (2004) *Proc Natl Acad Sci U S A* **101**, 7246-7251
26. Sali, A., and Blundell, T. L. (1993) *J Mol Biol* **234**, 779-815
27. Case, D. A. e. a. (2004) *University of California Sanfrancisco*
28. Ewing, T. J., Makino, S., Skillman, A. G., and Kuntz, I. D. (2001) *J Comput Aided Mol Des* **15**, 411-428
29. Jain, A. N. (2003) *J Med Chem* **46**, 499-511
30. Morris GM, G. D., Halliday RS, Huey R, Hart WE, Belew RK, Olson AJ. (1998) *J Comp Chem* **19**, 1639-1662
31. Merritt, E. A., and Murphy, M. E. (1994) *Acta Crystallogr D Biol Crystallogr* **50**, 869-873
32. Trent, J. O., Wang, Z. X., Murray, J. L., Shao, W., Tamamura, H., Fujii, N., and Peiper, S. C. (2003) *J Biol Chem* **278**, 47136-47144
33. Wang, J., Wang, W., Kollman, P. A., and Case, D. A. (2006) *J Mol Graph Model*
34. Jala, V. R., Shao, W. H., and Haribabu, B. (2005) *J Biol Chem* **280**, 4880-4887
35. Rao, J. V., Prakash, V., Rao, N. A., and Savithri, H. S. (2000) *Eur J Biochem* **267**, 5967-5976
36. Steeber, D. A., Engel, P., Miller, A. S., Sheetz, M. P., and Tedder, T. F. (1997) *J Immunol* **159**, 952-963
37. Ogilvie, P., Thelen, S., Moepps, B., Gierschik, P., da Silva Campos, A. C., Baggiolini, M., and Thelen, M. (2004) *J Immunol* **172**, 6715-6722
38. Baneres, J. L., Martin, A., Hullot, P., Girard, J. P., Rossi, J. C., and Parello, J. (2003) *J Mol Biol* **329**, 801-814
39. Lefkowitz, R. J. (1998) *J Biol Chem* **273**, 18677-18680
40. Pitcher, J. A., Freedman, N. J., and Lefkowitz, R. J. (1998) *Annu Rev Biochem* **67**, 653-692
41. Hubbell, W. L., Cafiso, D. S., and Altenbach, C. (2000) *Nat Struct Biol* **7**, 735-739
42. Hubbell, W. L., Altenbach, C., Hubbell, C. M., and Khorana, H. G. (2003) *Adv Protein Chem* **63**, 243-290
43. Farrens, D. L., Altenbach, C., Yang, K., Hubbell, W. L., and Khorana, H. G. (1996) *Science* **274**, 768-770
44. Haribabu, B., Zhelev, D. V., Pridgen, B. C., Richardson, R. M., Ali, H., and Snyderman, R. (1999) *J Biol Chem* **274**, 37087-37092
45. Menard, L., Ferguson, S. S., Zhang, J., Lin, F. T., Lefkowitz, R. J., Caron, M. G., and Barak, L. S. (1997) *Mol Pharmacol* **51**, 800-808
46. Swaminath, G., Deupi, X., Lee, T. W., Zhu, W., Thian, F. S., Kobilka, T. S., and Kobilka, B. (2005) *J Biol Chem* **280**, 22165-22171

47. Tunaru, S., Lattig, J., Kero, J., Krause, G., and Offermanns, S. (2005) *Mol Pharmacol* **68**, 1271-1280
48. Shin, N., Coates, E., Murgolo, N. J., Morse, K. L., Bayne, M., Strader, C. D., and Monsma, F. J., Jr. (2002) *Mol Pharmacol* **62**, 38-47
49. Gao, Z. G., Chen, A., Barak, D., Kim, S. K., Muller, C. E., and Jacobson, K. A. (2002) *J Biol Chem* **277**, 19056-19063
50. Quehenberger, O., Prossnitz, E. R., Cavanagh, S. L., Cochrane, C. G., and Ye, R. D. (1993) *J Biol Chem* **268**, 18167-18175
51. Hata, A. N., Lybrand, T. P., and Breyer, R. M. (2005) *J Biol Chem* **280**, 32442-32451
52. Blanpain, C., Doranz, B. J., Bondue, A., Govaerts, C., De Leener, A., Vassart, G., Doms, R. W., Proudfoot, A., and Parmentier, M. (2003) *J Biol Chem* **278**, 5179-5187
53. Colvin, R. A., Campanella, G. S., Manice, L. A., and Luster, A. D. (2006) *Mol Cell Biol* **26**, 5838-5849
54. Schwartz, T. W., Frimurer, T. M., Holst, B., Rosenkilde, M. M., and Elling, C. E. (2006) *Annu Rev Pharmacol Toxicol* **46**, 481-519
55. Altenbach, C., Yang, K., Farrens, D. L., Farahbakhsh, Z. T., Khorana, H. G., and Hubbell, W. L. (1996) *Biochemistry* **35**, 12470-12478
56. Zhou, W., Flanagan, C., Ballesteros, J. A., Konvicka, K., Davidson, J. S., Weinstein, H., Millar, R. P., and Sealfon, S. C. (1994) *Mol Pharmacol* **45**, 165-170
57. Liu, W., Eilers, M., Patel, A. B., and Smith, S. O. (2004) *J Mol Biol* **337**, 713-729
58. Scheer, A., Fanelli, F., Costa, T., De Benedetti, P. G., and Cotecchia, S. (1996) *Embo J* **15**, 3566-3578

Figure Legends

Figure 1: Leukotriene B_4 binding site in human BLT1: (A) *Schematic representation of human BLT1*: The boundaries of each transmembrane (TM), extracellular (ECL) and intracellular (ICL) domains are derived from the molecular dynamics modeled structure of BLT1. The amino acid residues involved in the ligand binding and activation process are shaded green and red, respectively. Mutated residues in ECL2 showing no affect on the ligand binding or signaling are shaded in pink.
(B) *LTB_4 docked structural model for BLT1 refined by restricted molecular dynamics (Methods)*: The seven transmembrane helices are colored TM1 (blue), TM2 (green), TM3 (yellow), TM4 (brown), TM5 (grey), TM6 (pink), TM7 (orange) and helix VIII red. LTB_4 is rendered as space-filled with carbon atoms colored dark grey, hydrogen atoms in white and oxygen atoms in red. (C) *The binding groove with LTB_4 bound:* Surface rendering of a cross section of BLT1 displaying the binding site with LTB_4 docked (ligand represented as thick sticks, carbon atoms- green, oxygen atoms- red and hydrogen atoms –white).

Figure 2: Characterization of LTB_4 binding site mutants in BLT1: (A) *BLT1 Ligand binding pocket*: Computational model of the BLT1 binding pocket with LTB_4 bound, obtained by a consensus docking protocol (Methods). The predicted hydrogen bonding and electrostatic interactions are shown for E185, Y102, N241, R156, T157, H94 and LTB_4 which stabilize the bound ligand in the pocket. Transmembrane helices III, IV, V, VI and ECL2 are shown with TM V rendered transparent. Hydrogen atoms are not displayed for clarity. (B) *Stable Expression of BLT1 and its mutants in 300.19 cells:* Indirect immunofluorescence staining of 300.19 cells (300.19 - grey) and 300.19 stably expressing BLT1 and the indicated mutants with 12CA5 mAb and FITC-conjugated goat anti mouse IgG.(C and D) *Saturation Ligand Binding:* Representative saturation binding curve and scatchard plot of $[^3H]$-LTB_4 binding to the 300.19 cells expressing BLT1 and Y102A. Data shown is representative of at least two independent experiments with triplicate measurements in each experiment. (E) *Competition Ligand binding:* Representative curves from one of three independent experiments of $[^3H]$-LTB_4 competition binding to the 300.19 cells expressing BLT1 or the indicated

mutants. (F) *Chemotaxis:* Ligand dependent chemotaxis of BLT1 or its mutants was measured by transwell filters as described in methods. Data are the mean ± SD of cells counted from two individual wells (counted four fields per well) that migrated to the lower chamber for each concentration from a representative experiment of at least three repetitions. The color scheme in the panels b, c and d is as follows: BLT1 - black; YN-AA (Y102A, N241A) – orange; Y102A – red; N241A – blue; E185A – purple and H94A – cyan.

Figure 3: Intracellular calcium release by BLT1 binding site mutants: 300.19 cells expressing BLT1 or mutants were loaded with Indo-1 and induced with various concentrations (0.1 nM-blue; 0.3 nM-red; 1.0 nM-green; 3.0 nM-purple; 10 nM-orange; 30.0 nM-grey; 100 nM-brown; 300.0 nM-black; 1000 nM-light blue; 3000 nM-pink) of LTB_4 and the Ca^{2+} mobilization was measured. Data in (A) BLT1 (B) Y102A (C) N241A (D) H94A (E) Y102A-N241A is representative of at least three independent experiments. (F) Percentage maximum calcium response of BLT1 and mutants as compared to BLT1 is an average of three independent experiments for each mutant.

Figure 4: Characterization of LTB_4 binding site mutants in ECL2 of BLT1: (A) *Chemotaxis:* Ligand dependent chemotaxis of BLT1 or its mutants was measured by transwell filters as described in methods. Data are the mean ± SD of cells counted from two individual wells (counted four fields per well) that migrated to the lower chamber for each concentration from a representative experiment of at least three repetitions. The color scheme in the panel A is as follows: BLT1 - black; R171A-R178A – pink; RT/AA (R156A-T157A) – green; R156A – brown; T157A – grey. (B, C, D, E) *Intracellular calcium release:* 300.19 cells expressing BLT1 mutants were loaded with Indo-1 and induced with various concentrations (0.1 nM-blue; 0.3 nM-red; 1.0 nM-green; 3.0 nM-purple; 10 nM-orange; 30.0 nM-grey; 100 nM-brown; 300.0 nM-black; 1000 nM-light blue; 3000 nM-pink) of LTB_4 and the Ca^{2+} mobilization was measured. Data in (B) R171A-R178A (C) R156A-T157A (D) R156A (E) T157A is representative of at least three independent experiments. (F) Percentage maximum calcium response of BLT1 and mutants as compared to BLT1 is an average of three independent experiments for each mutant.

Figure 5: Phosphorylation of BLT-1 and mutants: (A) ^{32}P labeled 300-19 cells expressing BLT1 or mutants (5×10^6 cells per sample) were incubated for 5 min with LTB_4 as indicated. Cells were lysed and immunoprecipitated with 3F10 antibody and analyzed by SDS-Polyacrylamide gel electrophoresis and phosphor imager as described in methods. The data for each mutant is representative of at least three independent experiments with WT BLT1 as control except for E185A, which was performed only once. (B) Integrated counts were plotted as fold over basal level of phosphorylation for BLT1 and each of the mutants.

Figure 6: Molecular models of Active and Inactive States of BLT1: *Superimposition of the predicted inactive (blue) and active (green) state structural models of BLT1*: (A) Lateral view of the structure of BLT1 outlining major helical movements along the vertical (y) axis. (B) Top view showing rotation of helices around y-axis vector and translation of helices in the x-z plane. Helix VIII and loops are not shown for clarity. LTB_4 is rendered as space-filled with carbon atoms-cyan, hydrogen atoms-grey and oxygen atoms-red.

Figure 7: Interactions in the Activation Core of BLT1 and Characterization of mutants: (A) Inactive and (B) active states of BLT1: The D64-N281 and D64-N36 interactions are formed only in the active state. Heavy atom to heavy atom distances are shown. (C) *Stable Expression of BLT1 and its mutants in 300.19 cells:* Indirect immuno fluorescence staining of 300.19 cells (300.19 - grey) and 300.19 stably expressing BLT1 and the indicated mutants with 12CA5 mAb and FITC-conjugated goat anti mouse IgG. *(D) Chemotaxis:* Chemotaxis of BLT1 and its mutants was measured by transwell filters as described in methods. Data shown is representative of at least two

independent experiments with duplicate measurements for each concentration and four fields in the hemocytometer were counted per well and averages were obtained.

Figure 8: Functional analysis of BLT1 activation Core Mutants: (A-D) *Calcium Mobilization:* 300.19 cells expressing BLT1 and mutants were loaded with Indo-1 and induced with various concentrations (0.1 nM-blue; 0.3 nM-red; 1.0 nM-green; 3.0 nM-purple; 10 nM-orange; 30.0 nM-grey; 100 nM-brown; 300.0 nM-black; 500 nM-light blue) of LTB_4 and the increase in fluorescence was measured as a ratio at wavelengths 405/490 nm. Data in (A) BLT1 (B) D64A (C) N281A is representative of at least three independent experiments. (D) Percentage maximum calcium response of BLT1 and mutants as compared to BLT1 is an average of three independent experiments for each mutant. (E) *Phosphorylation of BLT-1 and mutants:* ^{32}P labeled 300-19 cells expressing BLT1 or mutants (5×10^6 cells per sample) were incubated for 5 min with LTB_4 (100 nM) PMA (100 ng/ml) or buffer (control) as indicated. Cell lysates were immunoprecipitated with 3F10 antibody and analyzed by SDS-PAGE and phosphor imager as described in methods. The data for each mutant is representative of at least two independent experiments with WT BLT1 as control in each. (F) Integrated counts were plotted as fold over basal level of phosphorylation. (G) *LTB_4-induced co-localization of BLT1 and β-arrestin:* β-Arrestin-GFP (15 μg) is co-transfected along with either BLT1 or mutant receptors tagged with RFP (Mono) (25 μg) into RBL-2H3 cells. After the addition of LTB_4 (0-time), red and green fluorescence images were collected every 10 seconds for 15 min using appropriate filters as described in methods. With time, co-localization of β-arrestin-GFP and receptor RFP (yellow punctate distribution) is seen with both native and N36A mutant receptors, where as in D64A weak translocation of β-arrestin was observed. Ligand-induced β-arrestin translocation was absent in S277-79A and N281A mutants. The images are representative of at least 10 separate single cells analyzed for each mutant.

Table 1

	% Surface Expression[a]	EC 50 (nM)[b]	K_d (nM)[c]	B_{max}[c] sites/cell	Chemotaxis	Calcium Release (EC 50)[e]
BLT1	100	3.4	1.2 ± 0.17	17518 ± 450	3	0.427
H94A	218	31.6	nd	nd	100	25.3
Y102A	132.6	21.2	10.1 ± 3.5	22027 ± 2987	30	9.8
E185A	88.6	24.5	17.1 ± 5.3	23389 ± 4163	30	25
N241A	101.8	12.4	7.6 ± 2.1	19908 ± 2031	30	20
Y102A-N241A	121.6	56.6	58.9 ± 12.6	37418 ± 6876	300	279
R156A-T157A	212.8	ND	ND	ND	ND	ND
R156A	142	ND	ND	ND	ND	ND
T157A	110	2.6	2.6 ± 0.14	74018 ± 1553	3	0.84
R171A-R178A	140	5.5	1 ± 0.34	15575 ± 1559	3	0.32

Expression and functional properties of BLT1 and binding site mutants

a: Relative surface expression of BLT1 (100%) and mutants (Fig 2B)
b: EC50 measured from competition ^{3}H-LTB_4 binding assays (Fig 2E). Data is representative of three independent experiments with triplicate measurements in each.
c: K_d and B_{max} measured from saturation binding assays (representative examples in Fig 2C and D). Data is representative of at least two independent experiments with triplicate measurements in each.
d: The ligand concentration (nM) at maximum chemotaxis response (Fig 2F and Fig 4A)
e: The ligand concentration (nM) at 50% of the maximum calcium response (Fig 3F and Fig 4F)
nd: not determined; ND: No detectable binding, chemotaxis or calcium mobilization.

Table 2

	% Surface Expression[a]	EC 50 (nM)[b]	K_d (nM)[c]	B_{max}[c] sites per cell	Calcium Release[d] % activity at 10 nM
BLT1	100	3.4	1.2 ± 0.17	17518 ± 450	100
N281A	177	3.6	1.4 ± 0.29	52877 ± 3725	14.8
D64A	219	8.2	2.9 ± 0.63	36998 ± 2821	0.3
N36A	111	2	1.2 ± 0.37	48201 ± 4587	103.6
S277-79A	126	32.8	7.1 ± 2.8	29754 ± 5576	23.58

Expression and functional properties of BLT1 activation core mutants

a: Relative surface expression of BLT1 (100%) and mutants (Fig 7C)
b: EC50 measured from competition ^{3}H-LTB_4 binding assays. Data is representative of at least three independent experiments with triplicate measurements in each.
c: K_d and B_{max} measured from saturation binding assays. Data is representative of at least two independent experiments with triplicate measurements in each.
d: % of the maximum calcium response at 10 nM LTB_4 (Fig 8D)

Table 3

Residues	Positions					
(Type)	N1.50 *(N36)*	D2.50 *(D64)*	S7.45 *(S277)*	S7.46 *(S278)*	S7.47 *(S279)*	N7.49 *(N281)*
N	**1636**	46	504	32	9	**1027**
S	-	15	**221**	**489**	**111**	59
C	-	0	8	146	441	6
H	-	0	115	1	7	2
D	-	**1495**	4	17	8	213
E	-	44	11	13	28	6
Q	-	1	15	19	13	12
T	-	3	209	113	43	67
Y	-	3	10	14	33	30
R	-	0	33	12	17	15
K	-	1	22	26	17	16
Polar residues	1636	1608	1152	882	727	1453
Total residues	1636	1636	1636	1636	1636	1636
% conservation	100	98.3	70.4	53.9	44.4	88.8

Conservation of polar residues in class A GPCRs

The frequency of occurrence of the polar residues across 1636 class A GPCRs (www.GPCR.org) and percent conservation at congruent positions to that of the BLT1 (residue numbers shown in italics) activation core (The BLT1 residue types are in bold).

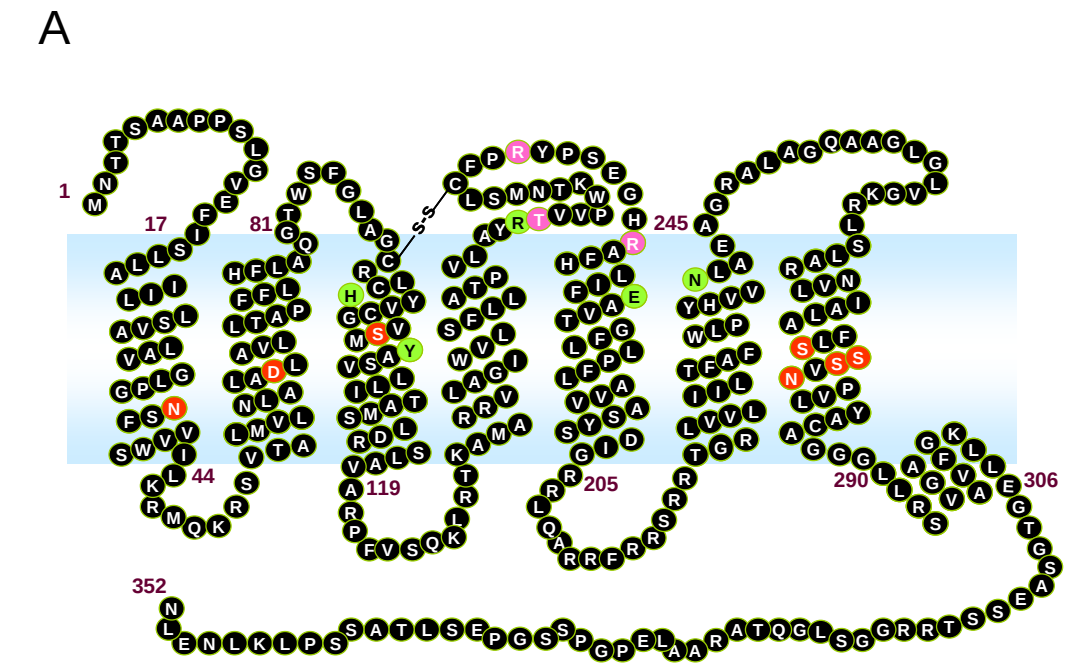

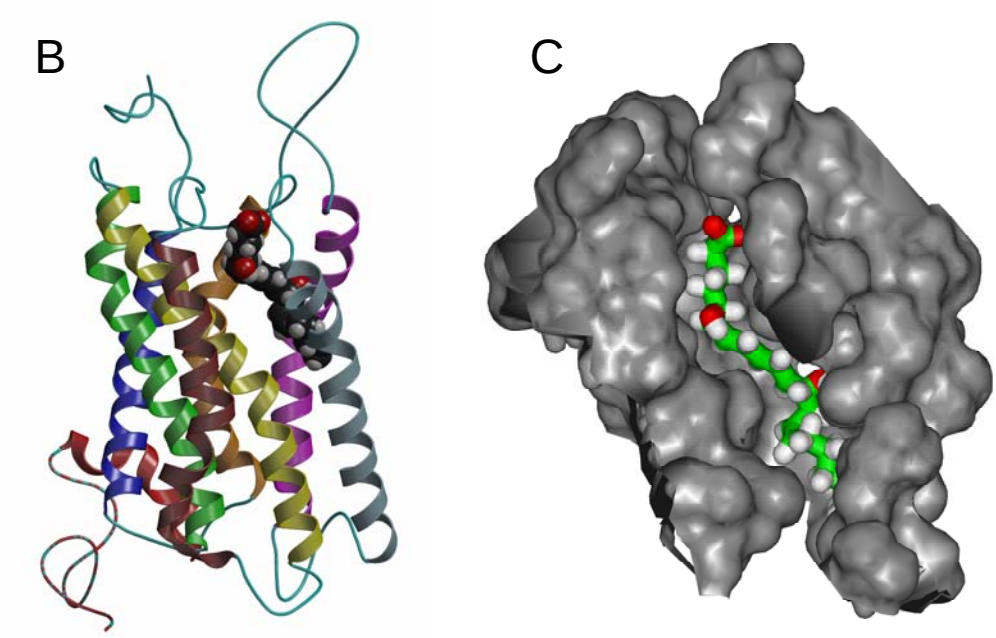

Figure 1

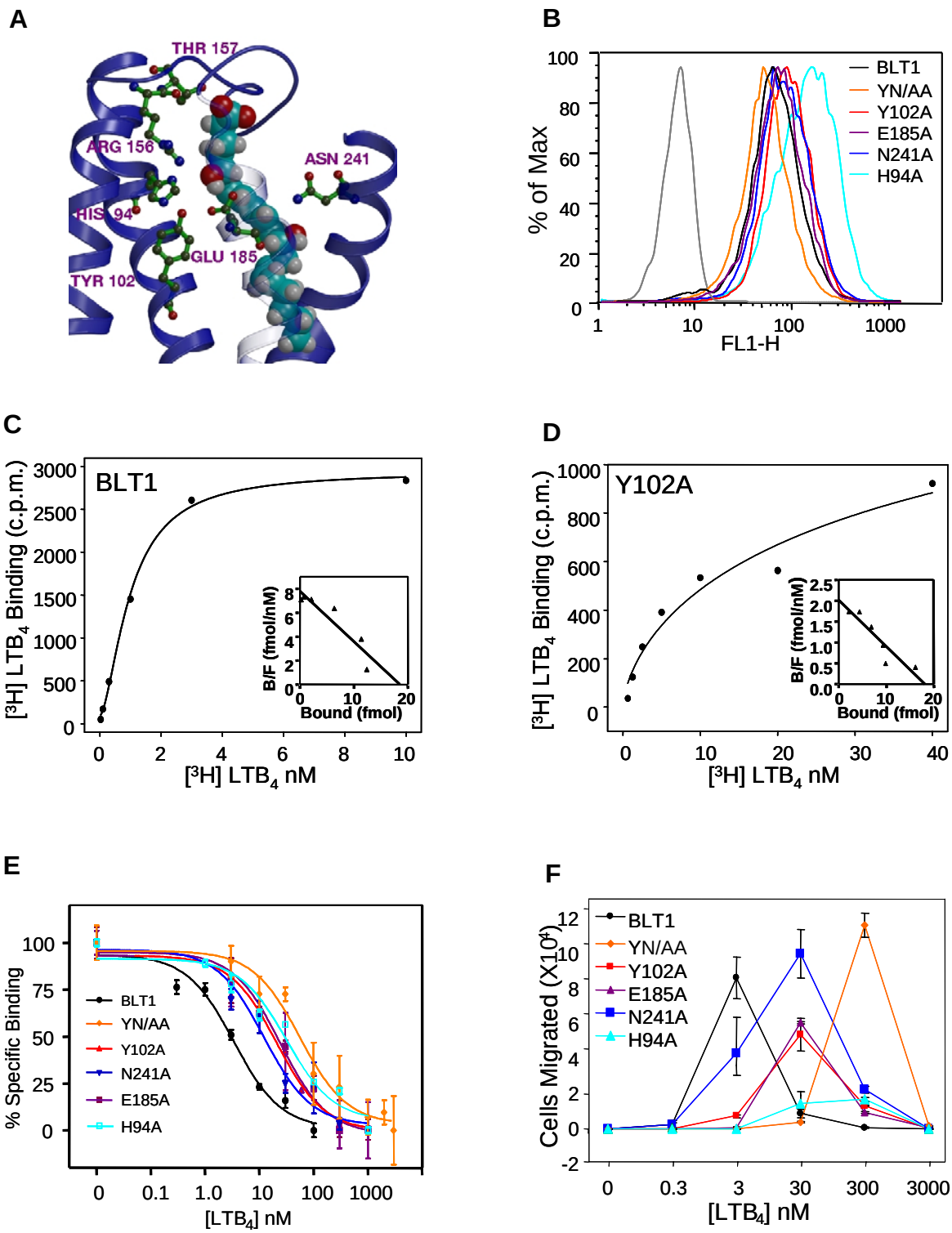
A
THR 157
ARG 156
ASN 241
HIS 94
GLU 185
TYR 102
B
% of Max
FL1-H
BLT1
YN/AA
Y102A
E185A
N241A
H94A
C
BLT1
[3H] LTB4 Binding (c.p.m.)
[3H] LTB4 nM
B/F (fmol/nM)
Bound (fmol)
D
Y102A
[3H] LTB4 Binding (c.p.m.)
[3H] LTB4 nM
B/F (fmol/nM)
Bound (fmol)
E
% Specific Binding
[LTB4] nM
BLT1
YN/AA
Y102A
N241A
E185A
H94A
F
Cells Migrated (X10^4)
[LTB4] nM
BLT1
YN/AA
Y102A
E185A
N241A
H94A

Figure 2

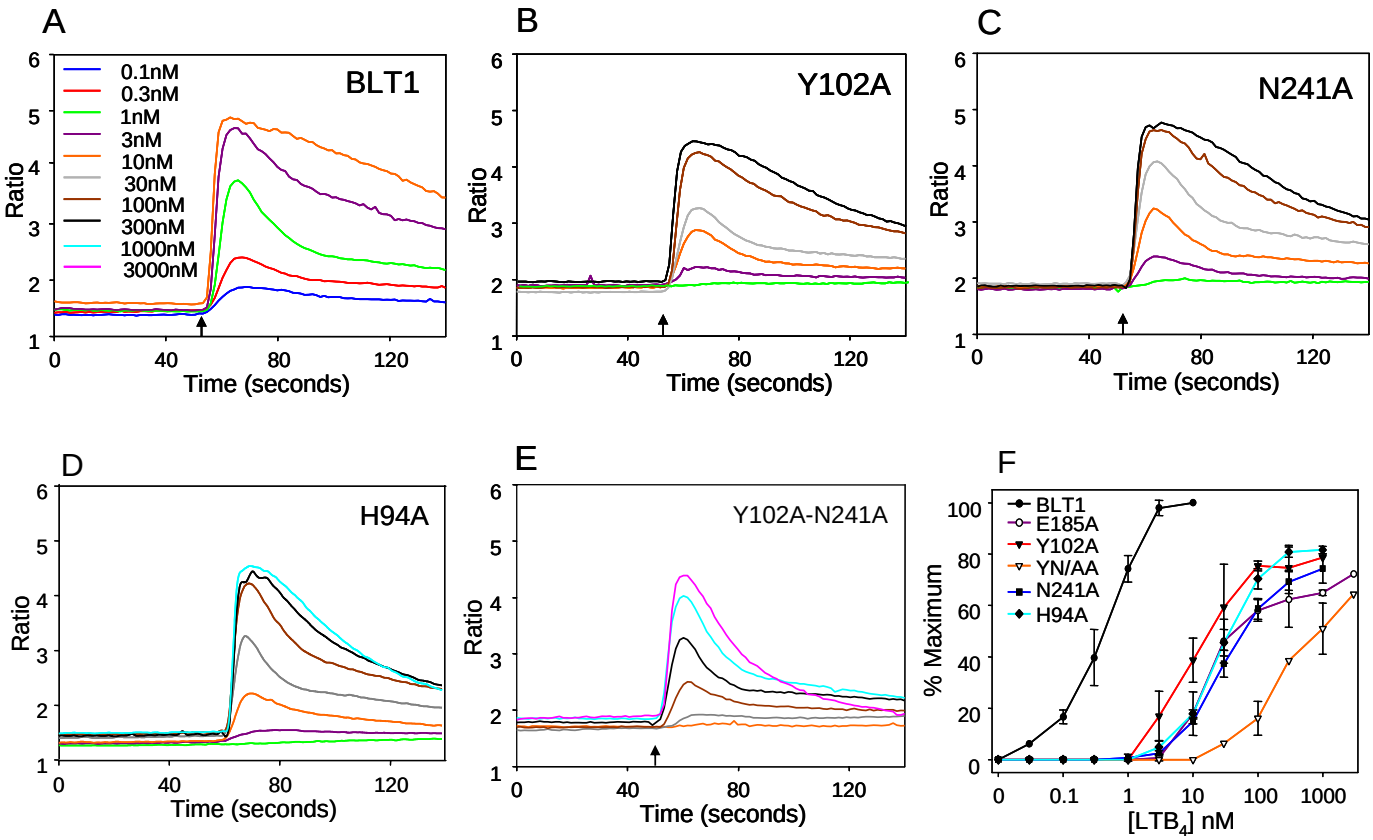
A
BLT1
0.1nM
0.3nM
1nM
3nM
10nM
30nM
100nM
300nM
1000nM
3000nM
Ratio
Time (seconds)
B
Y102A
C
N241A
D
H94A
E
Y102A-N241A
F
BLT1
E185A
Y102A
YN/AA
N241A
H94A
% Maximum
[LTB4] nM

Figure 3

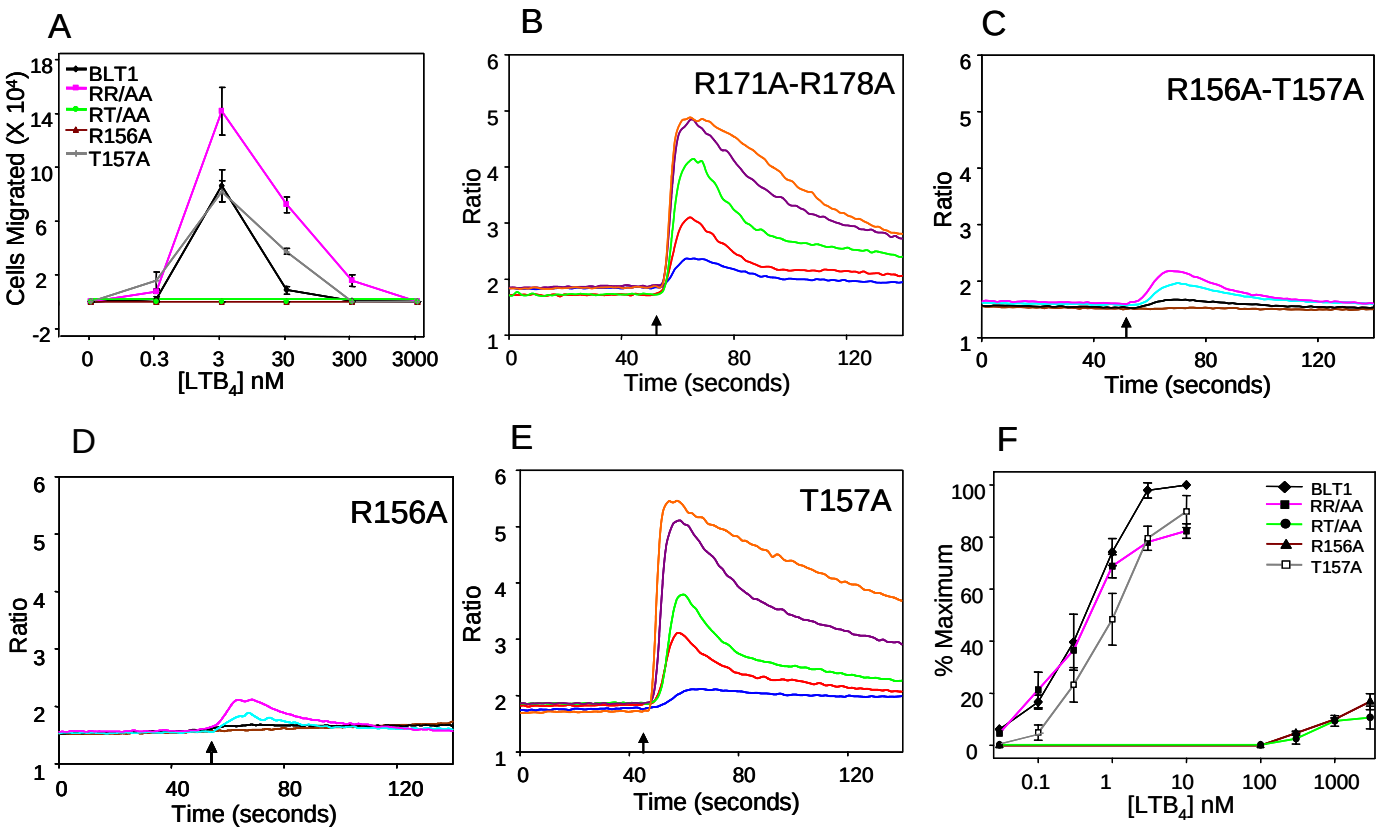
A
B
C
D
E
F
BLT1
RR/AA
RT/AA
R156A
T157A
Cells Migrated (X 10⁴)
[LTB4] nM
R171A-R178A
R156A-T157A
R156A
T157A
Ratio
Time (seconds)
% Maximum

Figure 4

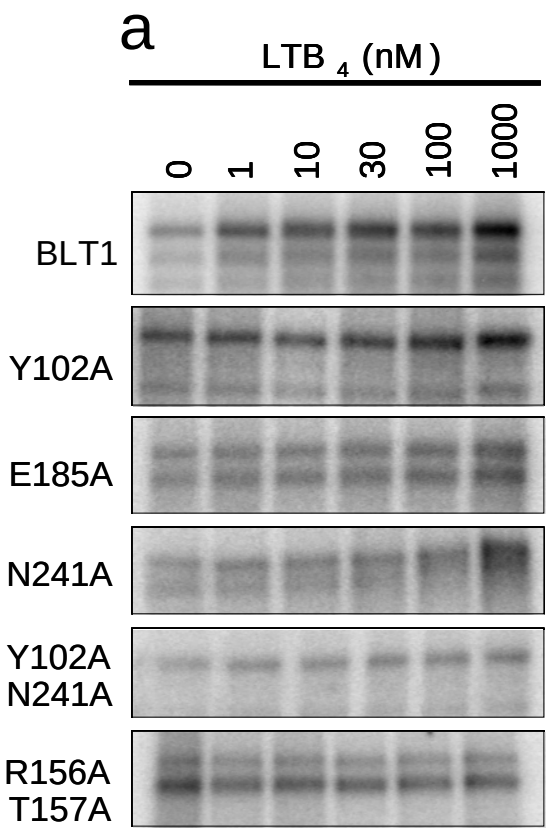
a
LTB 4 (nM)
0
1
10
30
100
1000
BLT1
Y102A
E185A
N241A
Y102A
N241A
R156A
T157A

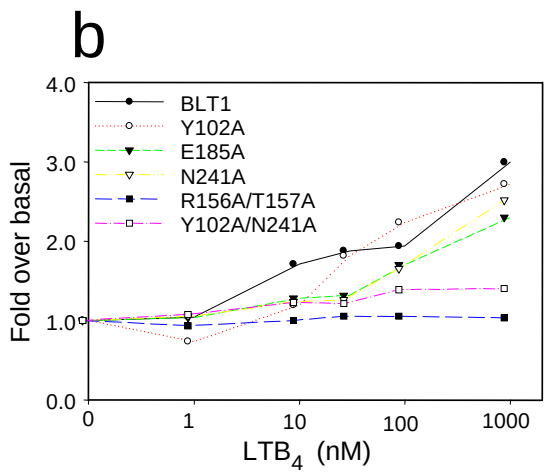
b
4.0
3.0
2.0
1.0
0.0
Fold over basal
BLT1
Y102A
E185A
N241A
R156A/T157A
Y102A/N241A
0
1
10
100
1000
LTB4 (nM)

Figure 5

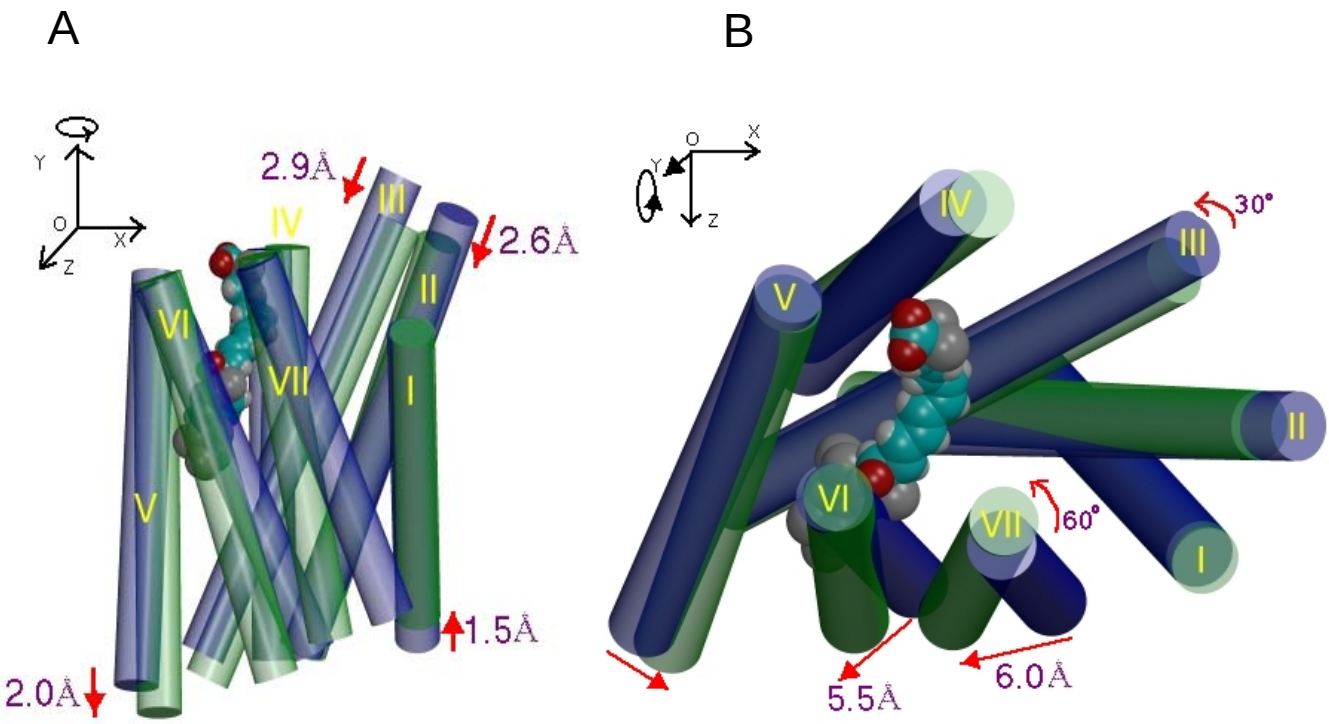

Figure 6

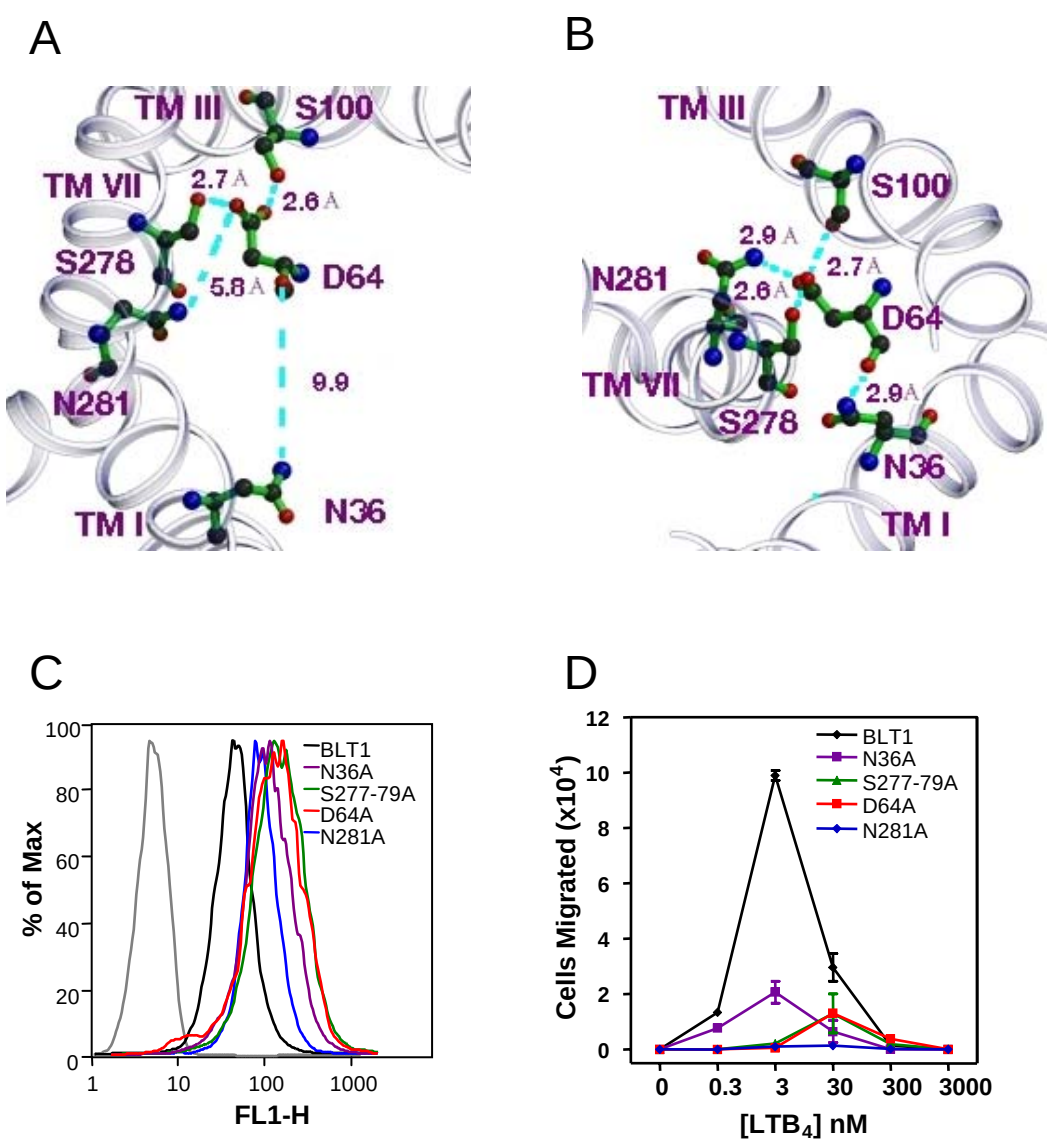
A
TM III
S100
TM VII
2.7 Å
2.6 Å
S278
5.8 Å
D64
9.9
N281
TM I
N36
B
TM III
S100
2.9 Å
2.7 Å
N281
2.6 Å
D64
TM VII
2.9 Å
S278
N36
TM I
C
100
80
60
40
20
0
% of Max
1
10
100
1000
FL1-H
BLT1
N36A
S277-79A
D64A
N281A
D
12
10
8
6
4
2
0
Cells Migrated (x10^4)
0
0.3
3
30
300
3000
[LTB4] nM
BLT1
N36A
S277-79A
D64A
N281A

Figure 7

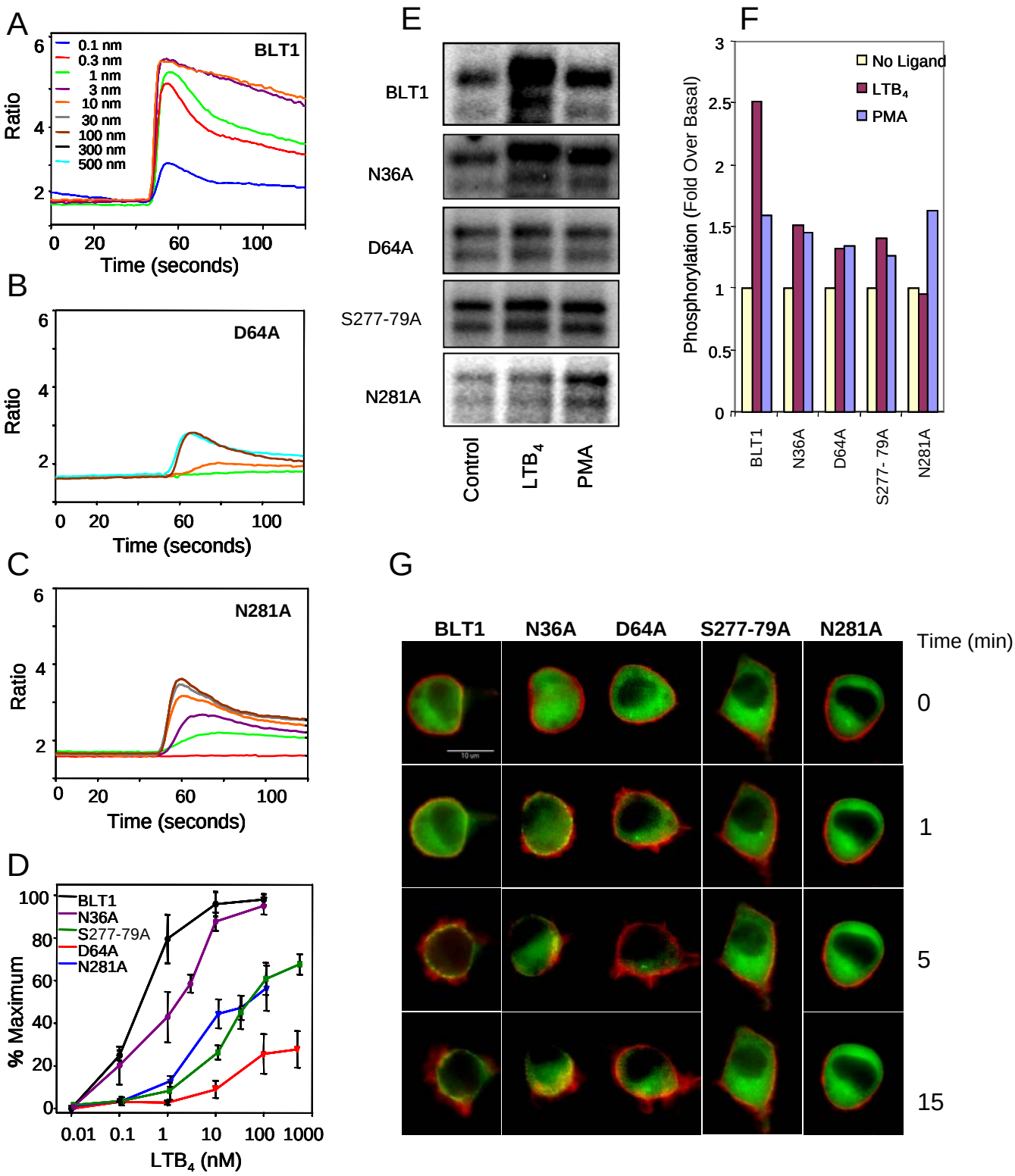
A
BLT1
0.1 nm
0.3 nm
1 nm
3 nm
10 nm
30 nm
100 nm
300 nm
500 nm
Ratio
Time (seconds)
B
D64A
Ratio
Time (seconds)
C
N281A
Ratio
Time (seconds)
D
BLT1
N36A
S277-79A
D64A
N281A
% Maximum
LTB4 (nM)
E
BLT1
N36A
D64A
S277-79A
N281A
Control
LTB4
PMA
F
No Ligand
LTB4
PMA
Phosphorylation (Fold Over Basal)
BLT1
N36A
D64A
S277- 79A
N281A
G
BLT1
N36A
D64A
S277-79A
N281A
Time (min)
0
1
5
15

Figure 8